Proceedings World Geothermal Congress 2020+1
Reykjavik, Iceland, April - October 2021

Apparatus for Studying the Corrosion Resistance of Alloys in High Temperature Geothermal Well Environment

Bente Cecilie Krogh[1], Lars Djupvik[1], Hans Husby[1], Marion Seiersten[2] and Morten Tjelta[2]

[1]Equinor ASA, Arkitekt Ebbels veg 10, 7005 Trondheim, Norway [2]Institute for Energy Technology, 2007 Kjeller, Norway

becek@equinor.com

Keywords: corrosion, laboratory testing, superheated steam, supercritical water, corrosion resistant alloys

ABSTRACT

An apparatus and experimental procedures for studying the corrosion behaviour of commercial corrosion resistant alloys (CRA's) are described. Harsh environment in high temperature geothermal wells was tried simulated with a field-relevant test fluid at low pH, temperature 350 °C and pressure 170 bars. Variations in pH during isochoric heating of 200 $g \cdot L^{-1}$ H_2O with HCl are shown. When starting with water at room temperature and pH 3, pH decreases slightly with increasing temperature before reaching a minimum close to 335 °C. The reason behind this behaviour is the competition between water dissociation, HCl dissociation and HCl partitioning (fractioning). HCl – which is commonly known as a strong acid – behaves as a weak acid at high temperature, and with increasing temperature the vapour phase becomes more acidic. The transition area of subcritical two-phase and supercritical water/superheated steam environment was of special interest since the corrosivity is expected to become more severe when liquid phase is present. The corrosion performance of materials at reducing conditions was investigated using rectangular, rod and C-ring samples. A 300-hour exposure test of Hastelloy C-276 (UNS N10276), Inconel 625 (UNS N06625) and Titanium grade 29 (UNS R56404) specimens are reported. Only the first two materials were available as C-rings test specimen. The samples were visually evaluated, and microstructure and corrosion products were further studied using SEM/EDS. The examination of specimens showed little or no corrosion. There were no cracks visible after C-ring testing of Hastelloy C-276 and Inconel 625. Plans for improved equipment design, characterization methods, and test procedure to obtain even more representative geothermal conditions in the future were outlined.

1. INTRODUCTION

One of the major technical challenges in high temperature geothermal wells is to identify suitable materials of construction for the geothermal environment. The choice of apparatus design and experimental procedures in the laboratory are important in order to simulate field conditions. Even if the laboratory equipment never can mimic all the field parameter and variations in operation of a well, as reviewed by Nogara and Zarrouk (2018), some of the most important parameters can still be addressed. Important corrosion rate promoters as low pH and temperature > 300 °C will be varied in the equipment described here. The laboratory corrosion test is planned to be a preparatory step before conducting more realistic field experiments. As first material candidates, some corrosion resistant alloys (CRA's) were evaluate and tested to map their stability window in harsh conditions typical for some high temperature geothermal wells.

The transition area of subcritical two-phase and supercritical water/superheated steam environment is of special interest since the corrosivity is expected to become more severe when liquid phase is present, Tjelta et al. (2019). Production of single-phase superheated steam is expected to keep the corrosion issues at a minimum. Even if a single-phase fluid is produced at steady state operation of a high temperature well, water will drop out during start-up, shut-downs and irregular production. Thorhallsson et al. (2018) experienced general and localized corrosion on UNS NO00625 at 350 °C in a flow-through reactor, probably due to liquid droplet transportation and condensation, see the experimental setup details in Thorhallsson et al. (2019). When two-phase fluid is present, the H^+ activity is important for the corrosion potential. To make the laboratory test fluid more field-relevant, HCl was chosen to be added to the water fluid to give a low pH, first pH 3 before decreasing pH to 2 and 1 in later tests. Also, in the future, minor amounts of NaCl, H_2, CO_2 and H_2S will be added step by step to check the effect and interaction of geothermal species in a corrosion perspective. This will improve the similarity between laboratory conditions and a geothermal reservoir.

2. EXPERIMENTAL

The experimental approach was an exposure of rectangular coupon, rod and C-ring samples in a pre-determined amount of fluid (water and add-ins) in a sealed batch autoclave and heat to the desired temperature. The pressure and phase distribution during heating could then be obtained by following the correct isochore (the constant density curve), as can be illustrated using NIST Chemistry WebBook, Lemmon (2017). The experimental work described herein is from a single test at pH 3, while simulations also were done for pH 2 and pH 1 conditions.

2.1 Low-pH in closed two-phase water/steam systems

In order to predict the variation in pH during heating of an autoclave, phase compositions were calculated along the 200 ($g \cdot L^{-1}$) water isochore using OLI Studio (2019). The amount of HCl required to reach the target pH at ambient conditions (25 °C and 1 atm) was calculated using the same software and included in the isochoric calculations. Parameters used in the calculations are summarized in Table 1.

Table 1: Summary of parameters used in the density calculations.

Label	pH (ambient)	Reactor *V* L	*m* H_2O g	*m* HCl g
pH1	1	1	200	$9.23 \cdot 10^{-1}$
pH2	2	1	200	$8.10 \cdot 10^{-2}$
pH3	3	1	200	$7.56 \cdot 10^{-3}$

The fluid in the test was deionized water, pH adjusted by use of HCl. The pH at start of the pH3 experiment was measured to be 2.7 at room temperature. Fluid samples were collected for future pH measurements by use of a combination electrode HACHE16M315 connected to a SensION+ PH31 pH-meter from HACH GSA.

2.2 Samples for corrosion measurement

Two types of metal coupons were exposed in the test. Both coupons and rods were ground to 1200 SiC and stored in a desiccator before and after the test. The rectangular coupons had the following dimensions: 20 mm wide by 30 mm long with square corners. The thickness somewhat varied for the three materials tested; Hastelloy C-276 (UNS N10276), Inconel 625 (UNS N06625) and Titanium grade 29 (UNS R56404) samples were 4.7, 4.8 and 2.9 mm thick respectively. The samples were placed on the bottom of the Hastelloy C-276 crucible in direct contact with the crucible material and completely submerged in water through the whole test. The other type of sample was rods of the same materials as the rectangular coupons. Dimension of the rod was 5 mm wide by 3 mm thick and the length was 255 mm. The length was chosen to ensure exposure to both phases along the whole length of the autoclave. The rods had a machined hole in one end which made it possible to hang them under the lid by use of Pt wires. Small alumina tubes were used to isolate the samples from the wire. There were a few millimetres clearance to the bottom of the crucible, and at least 5 cm of the lower part of the rod was submerged to the water phase throughout the test.

2.3 C-rings for environmental assisted cracking test

C-ring samples were included in the test to evaluate the susceptibility to environmentally assisted cracking (EAC) in accordance with standard practice ASTM G38 (2013). One sample of Hastelloy C-276 and one sample of Inconel 625 were included. The nominal sample dimensions were as given in **Table *2***.

Table 2: C-ring nominal sample dimensions.

	Hastelloy C-276 UNS N10276	**Inconel 625** UNS N06625
Width [mm]	10	9
Thickness [mm]	2.5	1.9
Outer diameter [mm]	25	19

The samples were tested with a fixed deflection, i.e., in constant strain. A screw going through the C-rings, with nuts on the ends, was used to compress the C-rings as described in ASTM G38. The screws and nuts were made of the same materials as the C-rings to avoid any galvanic effects. The desired reductions in C-ring outer diameters were calculated using the analytical framework in ASTM G38 for linear elastic materials. The desired deflections were calculated with basis in the testing temperature. The deflections were selected so that the circumferential stress at testing temperature would be 110% of the yield strength (YS), i.e., the samples were loaded to provide slight plastic deformation. When exceeding the proportional limit, the framework in ASTM G38 is no longer valid, but calculating in this way would provide a small amount of plastic strain for both samples. Testing in the plastic regime should ensure that the samples were sufficiently stressed for EAC to occur if the conditions were critical.

Since both the C-rings, bolts and nuts were made from the same materials – with equal thermal expansion coefficients – the strain on the samples would be independent of temperature variations. However, since the material YS for the tested materials decreases with increasing temperature, the necessary deflection to give the desired strain at testing temperature (350 °C) did not create plastic deformation at room temperature (RT). A moderate decrease of Youngs modulus (E-modulus) did not change this behaviour. Plastic deformation would therefore take place during the temperature rise at test start-up. In this way, the samples would not have reduced stress due to relaxation prior to testing. The mechanical properties of the two materials at RT and 350 °C are given in **Table *3***. The test deflections gave stresses of ~80% of Rp0.2 for Hastelloy C-276 and ~94% of Rp0.2 for Inconel 625 at RT. How the stress changes on increasing temperature for a fixed deflection/strain is illustrated in **Figure *1***.

Table 3: Mechanical properties with temperature. E-modulus data from BSSA (2019) and YS data from Gruben et al. (2019).

	Hastelloy C-276 UNS N10276	**Inconel 625** UNS N06625
YS (Rp0.2) at RT [MPa]	347.5	447.5
YS (Rp0.2) at 350 °C [MPa]	227.0	342.5
E-modulus at RT [GPa]	189.4	191.3
E-modulus at 350 °C [GPa]	170.9	172.0

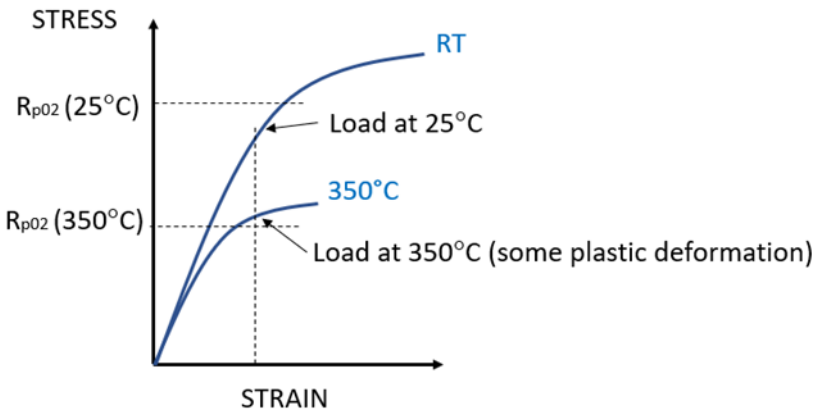

Figure 1: Illustration of the effect of the temperature increase on C-ring stress for a fixed deflection/strain.

The initial and final outer diameter of the C-rings were measured by a digital calliper. The C-ring samples were cut from hollow tubes using the outer diameters and wall thicknesses as the C-ring dimensions, **Table *1***. There was no further preparation of the sample surfaces. Before testing, the C-rings, including nuts and sticks, were rinsed in soapy water, tap water, distilled water and sonicated in acetone. The samples were mounted and strained. After straining, the C-rings were examined in the light microscope at 25x magnification at the outer surface and sides for any pre-existing cracks. The samples were spray-rinsed with acetone before installation in the autoclave. The C-rings were placed at the bottom of the autoclave with the surface in tension pointing upwards.

After testing, the samples were spray-rinsed with distilled water and ethanol immediately after extraction. The samples were then investigated in the light microscope at 25x magnification on the outer surface and sides – while in tension – for any cracks that had formed during testing. Then, the C-rings were relieved from stress by removing the nuts and the outer diameter of the C-rings were measured to see if it had decreased due to relaxation, plastic deformation or cracking during the test.

2.4 Apparatus and test procedure

The experimental setup and batch autoclave details can be seen in **Figure *2*** and Figure 3. A crucible (15 cm long and 9 cm wide) made of Hastelloy were placed inside the autoclave to avoid corrosion of the autoclave during heating up. 342 ml deionized water with HCl (pH 2.7) and 200 $g \cdot L^{-1}$ was added to the crucible. The samples were then placed on the bottom before the crucible was placed inside the autoclave. The rod samples were mounted under the lid using Pt-wires and isolation pieces of alumina tubes. The rods hang vertically straight down into the water phase but did not touch the sides or the bottom of the crucible or autoclave. The autoclave was closed and pressurized and depressurized ten times before leak testing at 150 bars. The water phase was then purged with N_2 through the dip tube (Figure 3) under no pressure and at room temperature (RT) overnight. The autoclave was then heated up 0.5 °C/min to 350 °C, where the pressure reached 170 bars. After 270 hours at 350 °C the autoclave was cooled to RT at around 0.8 °C/min. To avoid condensation during cooling, the gas phase was removed gradually by depressurizing through the gas relief valves on the heated outlet line (**Figure *2***). The condensed steam was then directed down into a knock-out drum after passing a cooling loop, no steam or water escaped to the vent. The condensed water was collected after test and stored in glass bottles for future analysis.

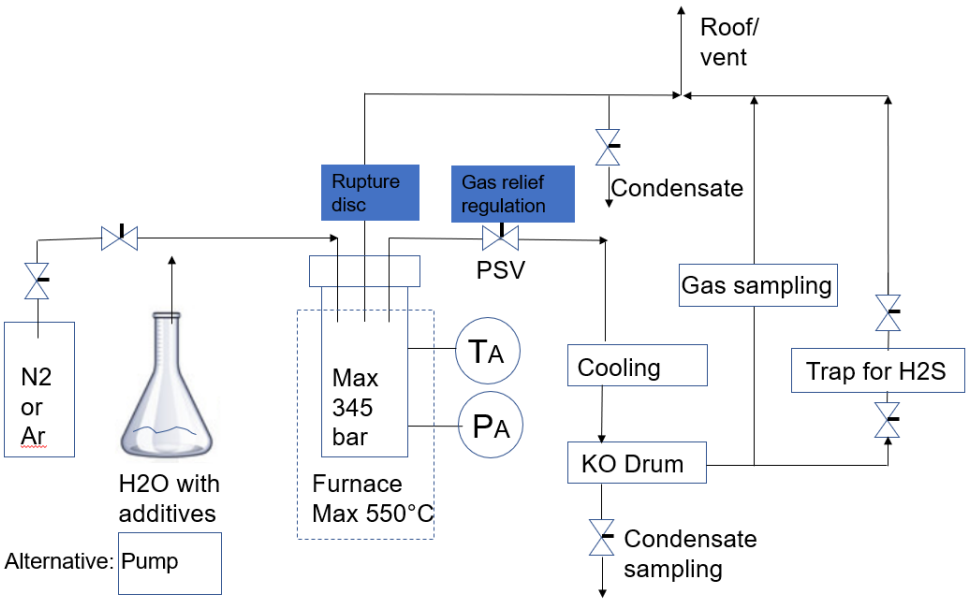

Figure 2: Flow diagram of experimental setup with sealed batch autoclave. During testing in- and out-valves were closed.

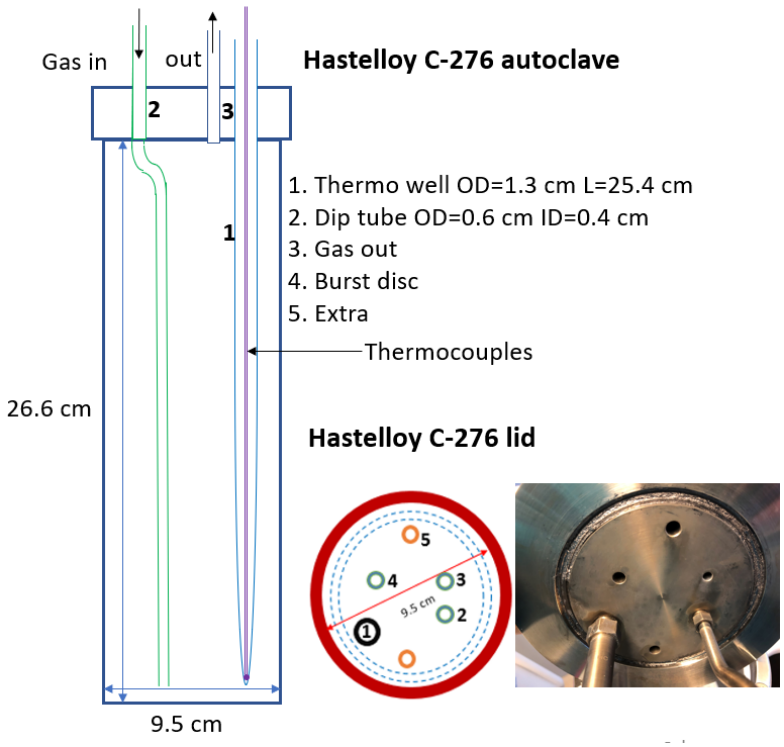

Figure 3: Details of the 1.8 L batch autoclave. Design temperature and pressure is 550 °C and 345 bars. A crucible (15 cm long, 9 cm wide) made of Hastelloy were placed inside the autoclave to avoid corrosion of the autoclave during heating up. The rod samples were mounted under the lid seen at bottom right.

2.5 Characterization methods

The stereo microscope used was an Olympus SZX12-TBI from Japan. A Scanning Electron Microscope, SEM, Quanta FEG 650 from FEI Company Netherlands, was used to collect some representative images of the samples. HV (high voltage) was set to 15 keV, working distance 10 mm and spot size 5.0. To identify the elemental composition, Energy-dispersive X-ray spectroscopy (EDS) is suitable to give chemical analysis of ca. 1 μm^2 area. Bruker Corporation, Nano GmbH, Germany has supplied an XFlash Detector 5040 for this purpose.

3. RESULTS AND DISCUSSION

3.1 Water and gas phase variations in an isochoric system

For all calculations, the mixed solvent electrolyte (MSE) model was used. Initial test calculations showed that the MSE model gave better agreement with available literature data, Cooper (2008), for the water dissociation constant than did the traditional aqueous model. Up to around 200 °C the two models give essentially identical results, while at higher temperature (lower density) the MSE model would be the best choice. Note, however, that also the MSE model should be used with caution when approaching the critical temperature.

Plotting isochores is a convenient way to estimate how the conditions in a closed autoclave evolve during heating. The overall fluid density in an autoclave of 1 L filled with 200 g H_2O at ambient conditions will have a constant system density of 200 $g \cdot L^{-1}$ at any temperature. In practice, one would typically purge the system with N_2 to remove oxygen. The small amount of N_2 (< 1 $g \cdot L^{-1}$ at ambient conditions) needed was included in some test calculations but did not have any significant effect on the calculated values. It was found, however, that the presence of N_2 made it difficult to obtain convergence at higher temperatures – thus, N_2 was omitted from further calculations.

Figure 4 shows how the pressure develops during isochoric heating of a 200 $g \cdot L^{-1}$ H_2O autoclave. The red line shows data for pure water obtained from the NIST database, Lemmon (2017), and the black and green dashed curves show calculations performed using OLI for a system without and with HCl, respectively. From the curves we see that the calculations agree well with NIST data up to the critical temperature. Also, the relatively small amount of HCl added (< 0.5 wt. %, cf. **Table *1***) does not affect the pressure.

Figure 5 shows the variation in pH during isochoric heating of 200 $g \cdot L^{-1}$ H_2O with HCl as stated in **Table *1***. With small amounts of HCl (i.e. the pH3 case), pH decreases slightly with increasing temperature before reaching a minimum close to 335 °C. For the pH2 case, the pH increases slowly towards 300 °C, before it starts rising more rapidly upon further increasing the temperature. In the pH1 case, pH increases relatively slowly towards around 275 °C before a sharper increase is observed. The reason behind this behaviour is the competition between water dissociation, HCl dissociation and HCl partitioning (fractioning). For water, the dissociation constant increases with increasing temperature until it reaches a maximum around 300 °C. HCl, on the other hand, has a dissociation constant that decreases with increasing temperature, Tjelta et al. (2019). In other words, the proton activity from H_2O alone increases with increasing temperature (to the point of maximum), while the activity of protons from dissociated HCl decreases with increasing temperature. HCl – which is commonly known as a strong acid – behaves as a weak acid at high temperature, Kritzer (2004). The tendency of HCl to fractionate favourably to the gas phase, Liebscher (2010), with increasing temperature also contributes somewhat to a decrease in the liquid pH. A consequence is that the vapour phase becomes more acidic. Figure 6 shows the molar fractions in the respective phases and the effect on pH due to some HCl loss to the gas phase upon heating.

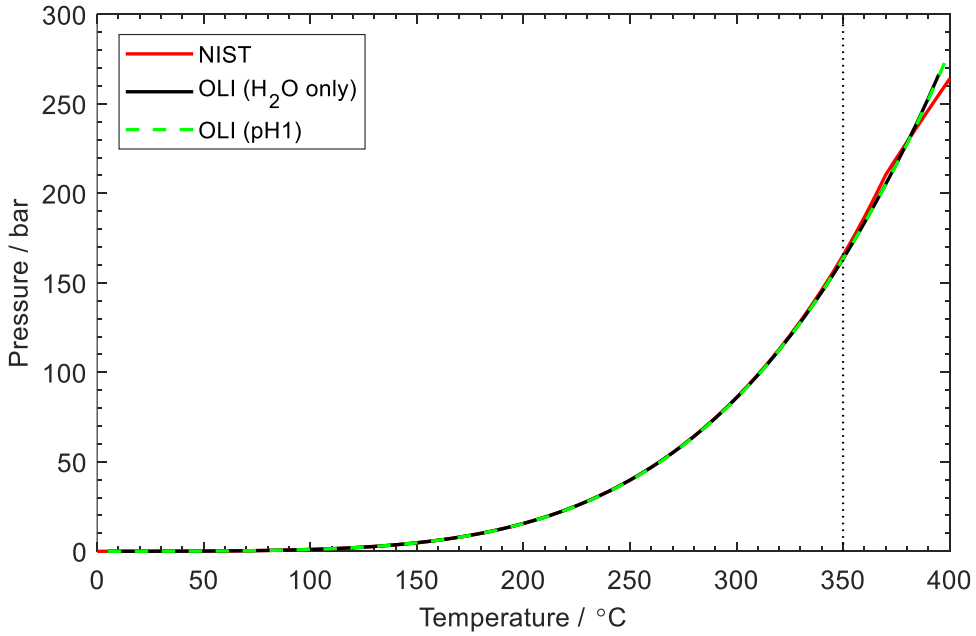

Figure 4: Pressure as a function of temperature for the 200 g L^{-1} H_2O isochoric system, representing heating of a closed autoclave. The red line shows data from the NIST database, and the black line shows values as calculated using OLI. The green dashed line shows the pressure during heating of an autoclave (1 L) with 200 g water and HCl to give pH 1, according to Table 1.

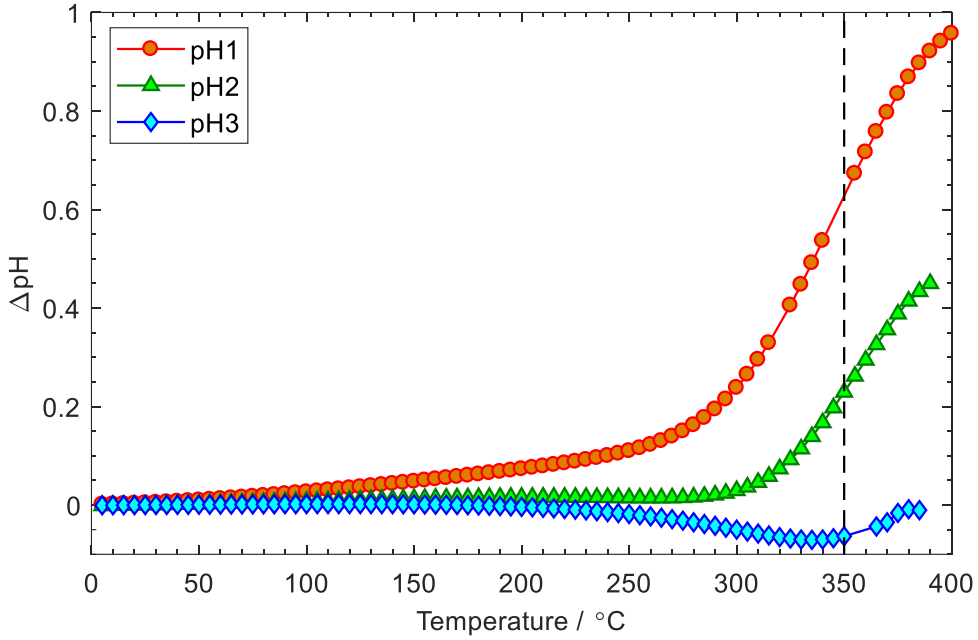

Figure 5: Variation in pH during isochoric heating of water with HCl according to Table 1. Filled symbols mark the calculated data points. The vertical dashed line indicates the temperature above where results should be used with caution.

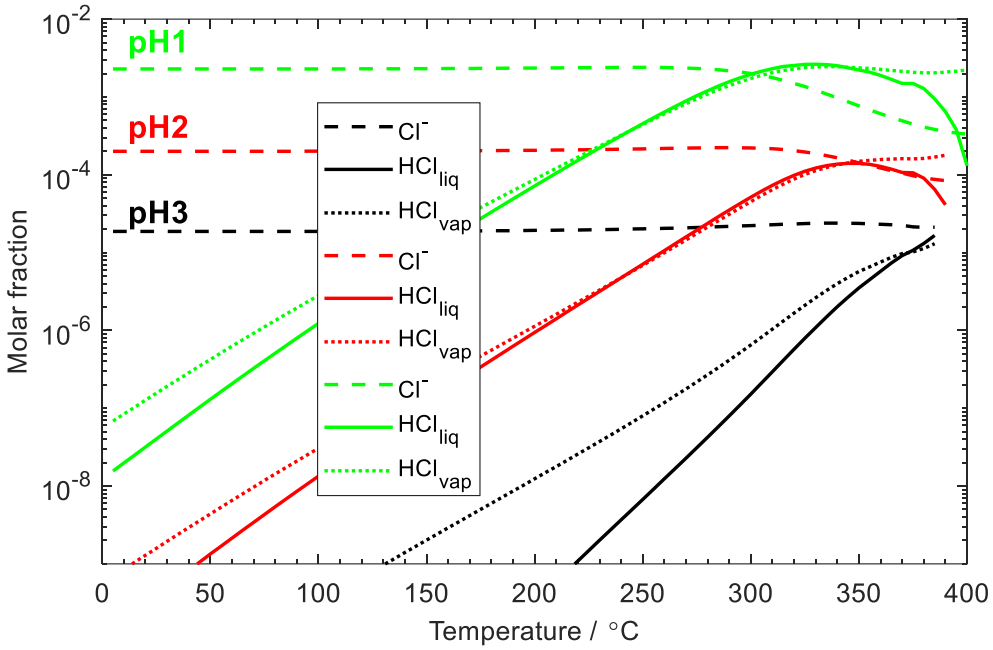

Figure 6: Variation in molar fraction of HCl in water (HCl_{liq}) and gas phase (HCl_{vap}) during heating of water with HCl according to Table 1. At temperatures above 350 °C the results should be used with caution.

3.2 Corrosion rate measurement

The Hastelloy C-276 (UNS N10276), Inconel 625 (UNS N06625) and Titanium grade 29 (UNS R56404) specimens showed low general corrosion, and there was no sign of localized corrosion on the surfaces. However, the morphology of the surface exposed to the water phase, interphase and steam phase was slightly different as shown in Figure 7. The test condition at pH 3 and test period of 300 hours will be used as basis for comparison for more corrosive conditions in future tests.

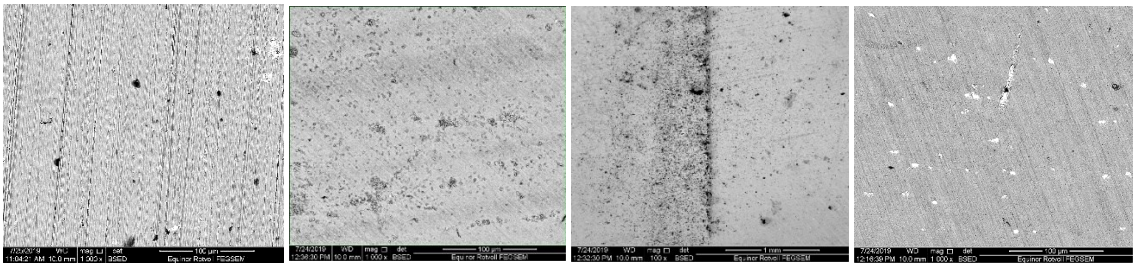

Figure 7: Backscatter SEM images showing morphologies of Inconel 625 rod sample surface as unexposed, exposed in the gas phase, interphase and water phase respectively. The image no. 3 in line (interphase) was magnified 100x, the other three 1000x.

EDS analysis showed that the darker spots at image no. 2 in Figure 7 (exposed in the gas phase) were rich in niobium, oxygen and possible carbon, titanium and molybdenum. The lighter spots on the water phase exposed surface (no. 4) were also rich in niobium and oxygen. Here only Inconel 625 rod alloy is shown, later surface and cross section of all samples will be examined in more detail. To find roughness of initial samples surface texture and eventual initial pitting development on exposed samples, a surface topography profiler could be used. Corrosion products could be analysed by XRD to give more accurate phase composition. An eventual galvanic effect due to contact between samples and the metal crucible will also be addressed in later runs.

The condensed gas phase was collected at room temperature after the test and will be characterized later. For instance, the content of metal ions and pH are of interest since depletion of reactants and eventual cross-contamination between different corroding specimens could give underestimated corrosion rates in a sealed autoclave system. The solution volume to specimen surface area ratio could be a critical factor. It can be advantageous to limit the ratio to be no less than 30 mL/cm^2. By using the equation given by Nogara and Zarrouk (2018), the ratio value was found to be under 4 mL/cm^2 in the test described here. To avoid decreasing corrosion rates over time, it should be considered to limit the test time and/or number or size of samples, another option could be to install a recirculating or flowing setup with fluid replenishment in future tests.

3.3 Environmental assisted cracking test

There were no cracks visible at 25x magnification on either of the two C-ring samples when examined after the autoclave test while still in tension. There were no loose corrosion products that could be considered to obscure cracks. The samples were somewhat discoloured. The Hastelloy C-276 sample had a blue/grey discoloration, while the Inconel 625 had a more colourful shine as seen in Figure 8.

The outer diameters of the C-ring samples decreased by 0.050 mm for the Hastelloy C-276 and 0.017 mm for the Inconel 625 samples as measured after testing compared to before. It is not certain whether the diameter reductions were due to stress relaxation at the high temperature, plastic deformation, or both.

Figure 8: Hastelloy C-276 and Inconel 625 samples after autoclave test at 350 °C.

It should be mentioned that when compressing the C-rings the accuracy was determined by the combined accuracy of the digital calliper and the operator, with the operator as the largest source or error. The C-rings were generally small, and the target reductions in outer diameters were only 0.25 and 0.29 mm for the Hastelloy and Inconel samples, respectively, leaving the exact testing stresses/strains somewhat uncertain. For future testing it will be considered to increase the diameter of the C-rings: by doubling the outer diameter, the required diameter reduction for a given stress is then increased by a factor of approximately four (given that the wall thickness is kept constant). Given that no cracks were visible at the outer surfaces or sides of the C-rings after testing, it will be considered to reuse the C-rings in tests with more severe conditions.

3.4 Visual inspection of equipment after test

Both the autoclave and the crucible used in the testing were made of Hastelloy C-275 alloy, and they both were discoloured from metallic to a deep brown-blue colour during the test. The autoclave had been through five initial test runs with same amount of pure deionized water to temperatures between 300 °C and 440 °C. The dark oxide layer formed is expected to protect the autoclave from

harmful corrosion test environment in future tests. The crucible can be replaced if it gets too corroded. The inner area of tubes and the inner passages through the lid were checked for corrosion products and pits by use of a snake inspection camera with light, and this type of examination will be a part of future test procedures.

4. CONCLUSIONS

Harsh environment in high temperature geothermal wells was simulated by a field-relevant test equipment at pH 3, temperature 350 °C and pressure 170 bars. Variations in pH during isochoric heating of 200 $g \cdot L^{-1}$ H_2O with HCl are shown. When starting with water at room temperature and pH 3, pH decreases slightly with increasing temperature before reaching a minimum close to 335 °C. The reason behind this behaviour is the competition between water dissociation, HCl dissociation and HCl partitioning (fractioning). HCl – which is commonly known as a strong acid – behaves as a weak acid at high temperature, and with increasing temperature the vapour phase becomes more acidic.

The corrosion performance of materials at reducing conditions was investigated using rectangular, rod and C-ring samples. An exposure test of Hastelloy C-276 (UNS N10276), Inconel 625 (UNS N06625) and Titanium grade 29 (UNS R56404) specimens showed little or no corrosion. Some spots of possible corrosion product enriched in niobium and oxygen were found on the surface of Inconel 625 alloy. There were no cracks visible on the C-ring samples made of Inconel 625 and Hastelloy C-276 after the test. There were no loose corrosion products that could be considered to obscure cracks. Plans for improved equipment design, characterization methods, and test procedure to obtain even more representative geothermal conditions in the future were outlined.

ACKNOWLEDGEMENTS

The Research Council of Norway's Innovation Project for Industry under grant agreement No 269399 to the HOTCASE project. The European Union HORIZON 2020 under grant agreement No 654497 to the GEOWELL project. Thanks to Equinor; Geir Haldogård and Sidsel Skauby for experimental work and Emil Edwin for advice during development of the methods. Thanks to Sintef and Bård Nyhus for advice on the C-ring testing.

REFERENCES

ASTM G-38-01: Standard Practice for Making and Using C-ring Stress-Corrosion Test Specimens, *ASTM International*, West Conshohocken, PA, available (07.18.2019): www.astm.org, (2013).

British Stainless Steel Association (BSSA): Elevated Temperature Physical Properties of Stainless Steels, available (07.18.2019): https://www.bssa.org.uk/topics.php?article=139, (2019).

Cooper, J.P. and Dooley, R.B.: Release on the Ionization Constant of H2O (R11-07), *The International Association for the Properties of Water and Steam (IAPWS)* (2008).

Gruben, G., Nyhus, B., Hoang, H.N., and Hellesvik, A.: Thermo-mechanical tensile testing, unpublished work in the *HotCaSe Project*, supported by Research Council of Norway (contract no. 269399), (2019).

Kritzer, P.: Corrosion in High-Temperature and Supercritical Water and Aqueous Solutions: A Review, *The Journal of Supercritical Fluids*, **29**, 1, (2004).

Lemmon, E.W., McLinden, M.O., and Friend D.G., in *NIST Chemistry WebBook, NIST Standard Reference Database Number 69*, Linstrom, P.J., and Mallard, W.G. Editors, National Institute of Standards and Technology, Gaithersburg MD, available (07.18.2019): https://webbook.nist.gov/chemistry/fluid/, (2017).

Liebscher, A., in *Frontiers in Geofluids*, Yardley, B., Manning, C., and Garven, G. Editors, (2010), 3.

Nogara, J. and Zarrouk, S.J.: Corrosion in Geothermal Environment, Part 2: Metals and Alloys*, Renewable and Sustainable Energy Reviews*, **82** (2018), 1347-1363.

OLI Systems Inc., v. 9.6, *OLI Studio* (2019).

Thorhallsson, A.I., Karlsdottir, S.N. and Stefansson, A.: Corrosion Testing of UNS N06625 in a Simulated High Temperature Geothermal Environment, NACE International, *CORROSION/2018*, paper no. 11058, Phoenix, Arizona (2018).

Thorhallsson, A.I., Karlsdottir, S.N. and Stefansson, A.: Corrosion Testing of UNS S31603 in Simulated HT Geothermal Environment at Boling, Superheated and Condensation Conditions, NACE International, *CORROSION/2019*, paper no. 13195, Nashville, Tennessee (2019).

Tjelta, M., Sæther, S., Krogh, B.C., and Seiersten, M.: Corrosion, Scaling and Material Selection in Deep Geothermal Wells – Application to IDDP-2, NACE International, *CORROSION/2019*, paper no. 13299, Nashville, Tennessee (2019).